Fracture Behavior of Short Fiber Reinforced Thermoplastics I. Crack Propagation Mode and Fracture Toughness

B. Z. JANG and Y. K. LIEU, *Department of Mechanical Engineering Material Science and Engineering Program Auburn University, Alabama 36849*

Synopsis

The fracture behavior of several short glass fiber reinforced thermoplastics has been studied. The fracture toughness of these materials may be related to local crack propagation mode, which is found to be highly rate dependent. At low test rates the crack growth in the reinforced polymers tend to follow a fiber avoidance mode, creating a greater area of new surfaces, which in conjunction with greater degree of interfacial debonding and fiber pullout friction leads to a higher fracture resistance. An increase in loading rate in general results in a more straight and flat crack path, as well as a lesser extent of fiber debonding and pullout. Therefore the fracture toughness is reduced although the frequency of fiber breakage is increased. The fracture behavior of these short fiber reinforced polymers appears to be dictated by the matrix properties when the loading rate is high.

INTRODUCTION

Short fiber reinforced thermoplastics (SFRP) are commercially important engineering materials, which may be processed by conventional techniques, such as injection molding, while providing an improvement in physical properties relative to those of the unfilled materials. They are being applied to automobiles because of their ease of fabrication (compared with continuous fiber composites), light weight, and economy.

However, the advantages are not gained without some sacrifice, the most obvious the increased processing difficulty relative to unreinforced plastics. This often leads to the formation of material defects, such as voids in the fabricated articles. A less obvious problem is the increased complexity of their mechanical behavior. Melt flow effects sometimes produce high levels of fiber orientation and anisotropy, which varies from point to point as well as through the thickness of typical molded parts. The properties normal to the predominant fiber orientation more closely resemble matrix and interface properties and can be very deficient in certain systems. Because of the very short fibers, even the properties in the most advantageous directions are influenced by the matrix and the interface to a much greater extent than in long fiber composites.[1-4] Unlike most long fiber composites, these materials can fail not only by fiber fracture, but often by matrix or by combined matrix and interface failure.

Perhaps because of this complexity, the fracture mechanism of the composites has not been fully understood. Several theoretical studies of the composite strength have been made on the basis of various postulated frac-

Journal of Applied Polymer Science, Vol. 30, 3925-3942 (1985)
 CCC 0021-8995/85/093925-18$04.00

ture mechanisms. Riley[5] studied the strength by modifying the formula of linear superposition of the strength of each component in the composite and showed that the failure will initiate when fiber stress reaches the ultimate tensile strength. A probabilistic approach was taken by Fukuda and Chou[6] to study the composite fracture, taking account of the fiber failure induced under the influence of the neighboring fiber end. Jaya[7] investigated the strength of a composite of which the failure is initiated by penny-shaped cracks in the matrix. Curtis et al.[8] demonstrated that the occurrence and accumulation of cracks at fiber ends greatly affect the mechanical behavior of the composite. Sato et al.[9] showed that the failure of glass-fiber–reinforced Nylon 6/6 proceeded in three stages: initiation of the interfacial cracks at fiber ends, propagation of such cracks along fiber sides, and crack propagation into the matrix leading to final material fracture.

In a study of the crack propagation modes in the injection-molded short fiber reinforced thermoplastics containing 30 or 40% by weight fibers, Mandell et al.[3,10] observed that the main crack tended to grow in a fiber-avoidance mode, bypassing regions of agglomeration of locally aligned fibers. The local mode of crack tip advance was found to vary with matrix ductility and bond strength. The effects of fiber content and loading rate or temperature on the crack propagation mode were not studied in these reports.[3,10] This work represents an important development in furthering our understanding of the failure behavior of SFRP. Depending upon the specific compositions of composites and on the loading conditions, the crack path has also been observed to proceed around the fiber/matrix interface (debonding) or through the fibers (fiber breakage). For instance, Schultz and Friedrich[11] reported that the fracture path of a PET-glass fiber composite was a function of temperature and loading rates. However, it is still not quite clear under precisely what conditions each of the above paths obtains, what the influence of the matrix is, or how the crack propagation mode is related to the macroscopic behavior. Research aiming at elucidating the roles played by the loading rate, matrix, and fiber arrangement in controlling the failure behavior of SFRP has been conducted. The results of crack propagation mode observation and fracture toughness measurements are presented here; the effects of material defects will be discussed in Part II.

EXPERIMENTAL

Materials and Sample Preparation

The materials used and their sources are listed in Table I. Nylon and polypropylene (PP) are semicrystalline polymers; polycarbonate (PC) and poly(ether sulfone) (PES) are amorphous. The PES material is a high-temperature polymer that is nominally brittle in uniaxial tensile tests. The other three unreinforced polymers are relatively ductile at room temperature. The tensile bar is a standard ASTM D638 Type 1. The compact tension bars follow the specification of the ASTM-E399 (Figure 1).[12] The tensile bars and flexural test bars were injection molded from a single end-gated mold. The rectangular plaques from which the compact tension specimens were machined were side-gated near a corner. Notches in compact tension spec-

TABLE 1
Materials and Supplier

Material designation	Matrix	Fiber	Manufacturer or compounder
N66ST	Rubber-toughened N66	—	duPont[a]
N66	Nylon 6/6	—	duPont[a]
N66-G13	Nylon 6/6	13% E-Glass	duPont[a]
N66-G33	Nylon 6/6	33% E-Glass	duPont[a]
PC	Polycarbonate	—	General Electric (GE)[b]
PC-G30	Polycarbonate	30% E-Glass	
PES-G30	Polyether sulfone	30% E-Glass	Wilson-Fiberfil[c]
PP	Polypropylene	—	Shell[b]
PP-G30	Polypropylene	30% E-Glass	Wilson-Fiberfil[c]

[a] All materials were manufactured and injection molded by duPont.
[b] Injection molded at Auburn University.
[c] Compounded and injection molded at Evansville Operations (Indiana) of Wilson-Fiberfil International.

imens were machined with a double-angle cutter; the radius at the notch root corners was approximately 0.06 mm. The notches were further sharpened by heavy-duty razor blade cuts or fatigue cracks.

The razor blade apparatus shown in Figure 2 was used to hold a blade in an MTS testing machine. The machine produces voltages from 0 to 10 V. Using a digital voltmeter, the load can be monitored while the machine ram with the sample is moved upward. When the razor blade just touches the sample, a voltage change can be noticed. With the stroke now being monitored, the ram can be manually moved to notch the sample. The notch depth can be accurately controlled; with the total stroke set to 10 mm, for instance, 1 V is then equal to 1 mm. The same MTS machine, which was servohydraulic driven, was used for a compact tension test. Tensile tests were conducted using this MTS machine as well as a floor model Instron.

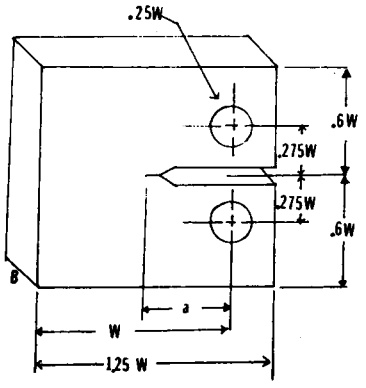

Fig. 1. The specimen geometry and dimensions used in the compact tension test.

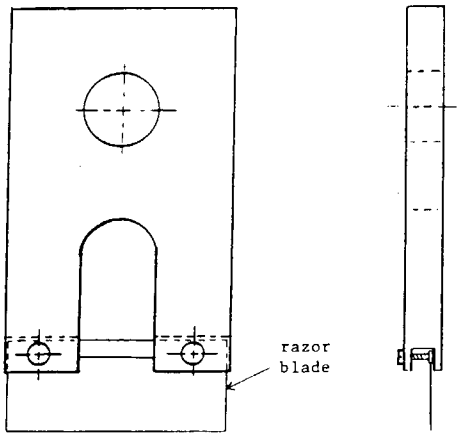

Fig. 2. The razor blade holder used in creating sharp starting crack.

Mechanical Tests

An ASTM D638 standard tensile test was conducted to understand the stiffness, strength, and ductility of each material. Flexural loading was used to propagate the existing crack. The rectangular bars used for crack propagation mode observation were carefully polished through normal metallographic procedures to ensure that the fibers and the growing crack tip could be clearly observed. Both the compact tension and flexural loading tests were performed at various strain rates. The strain rate was varied by selecting a series of standard crosshead speeds (0.01–50 in./min) of an Instron universal testing machine or by changing the ram (stroke) movement rate of the MTS system. An extremely high rate was facilitated by impact loading.

Microscopy

Both a light microscope (Zeiss) and scanning electron microscope (AMR Model 1000) were used to study the crack propagation mode in relation to the fiber morphology. Fracture surfaces of both flexural and compact tension specimens were examined by SEM to provide additional information on the failure mechanisms.

RESULTS AND DISCUSSION

Validity of Fracture Toughness Test

A standard test method for the plane strain fracture toughness K_{IC} of metals has been developed by ASTM, designated ASTM E399.[12] This method is restricted to two geometries: compact tension (CT) and three-point bending (TPB). The compact tension test was conducted throughout the present study.

The CT specimen containing a sharp crack was loaded to produce unstable crack extension. The fracture toughness K_c was determined by calculating

the value of stress intensity factor K_I at the load that produced unstable growth. This calculation was carried out without knowledge of the validity. The most straightforward method of determining the validity of the K_c value is to test specimens of different size and geometry. If K_c is a valid material property, it should be invariant as long as the same mode of growth is maintained. This approach to determining validity is tedious but may be used to justify more convenient methods. The validity of the tests is determined as follows:

The initial crack is made sufficiently sharp by precracking in fatigue at a low value of K_I prior to the fracture toughness test. We checked the difference in calculated K_c between fatigue precracking and sharp razor blade precracking. The difference was less than 8% for glass-fiber–reinforced Nylon and less than 6% for reinforced polyether sulfone. Razor blade precracking was therefore used throughout the study. A sharp starting crack is the first requirement for a valid K_{IC} test.

The force used in calculating K_I at fracture is determined from a force versus crack opening displacement (COD) curve to give the load corresponding to a 2% increase in crack length. This curve is also used to reject tests that sustain subsequent loads more than 10% higher than this value. This represents the second criterion. Most of our specimens, except rubber-toughened Nylon 6/6, pass this criterion.

The third criterion is that the quantity $S = 2.5\ (K_Q/\sigma_y)^2$ must be less than the crack length and the specimen thickness in order to have a valid K_{IC} test. K_Q is the candidate value of fracture toughness calculated from the load for the second step and an analytical expression of K_I in terms of the specimen geometry (K – calibration); σ_y is the yield stress in uniaxial tension at the corresponding rate and temperature. If S is too large compared with specimen dimensions, a larger size must be used and retested. With a thickness of ½ in., most of the unreinforced specimens do not satisfy this criterion.

Typical load-displacement curves obtained from CT tests are shown in Figures 3A–D for N66, N66ST, N66/G13, and N66/G33, respectively. Figure 3B indicates that the curve of rubber-toughened nylon does not meet the second criterion, nor does it meet the third one primarily because the value of K_c is proportional to $(1/\sigma_y^2)$. Rubber toughening has produced a lowering of nylon yield strength by an average of 35%. On the other hand, fiber reinforcements had increased the yield strength of N66 by 13% (13% fiber) and 56% (33% fiber), respectively. The extension rate dependence of the yield strengths of these materials is shown in Figure 4.

It may be noted that ASTM E399 suggests a specimen strength ratio R_{SC}, which is a dimensionless product and has the same value in any consistent system of units. R_{SC} can be a useful tool in comparing specimens' similar dimensions. R_{SC} is defined to be proportional to (P_{max}/σ_y) where P_{max} is the maximum load in the compact tension test.

It was found that the notch depth had little or no effect on the specimen strength ratio R_{SC} and fracture toughness K_Q (Table II) with the exception that, when the notch depth was very small, both K_Q and R_{SC} increased with increasing notch depth for PES-G30. Other materials studied appeared to be notch depth insensitive. The notch depth dependence of PC materials

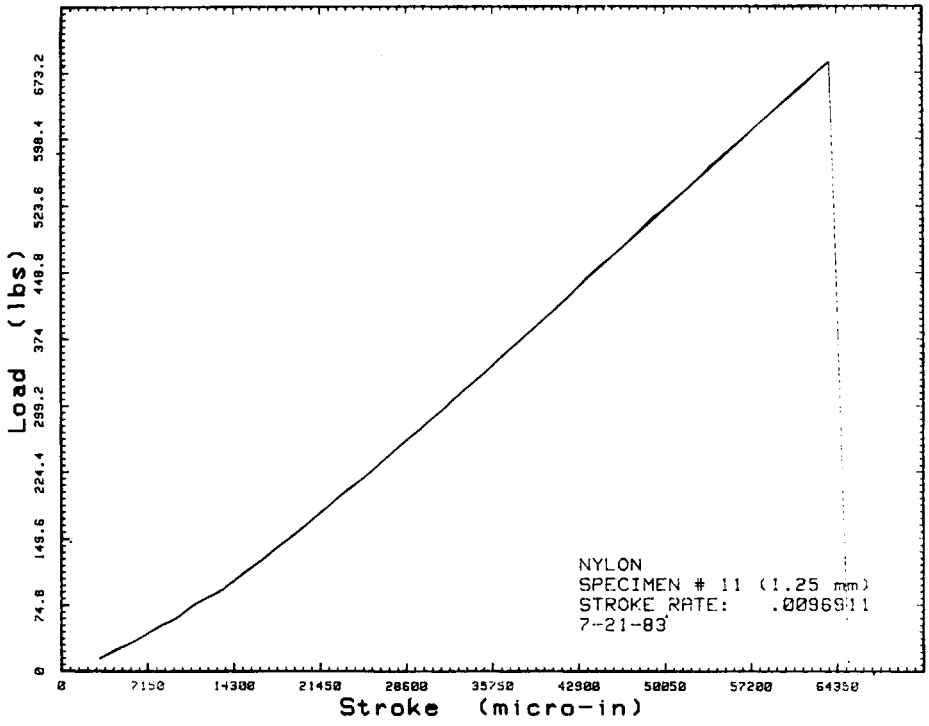

(a)

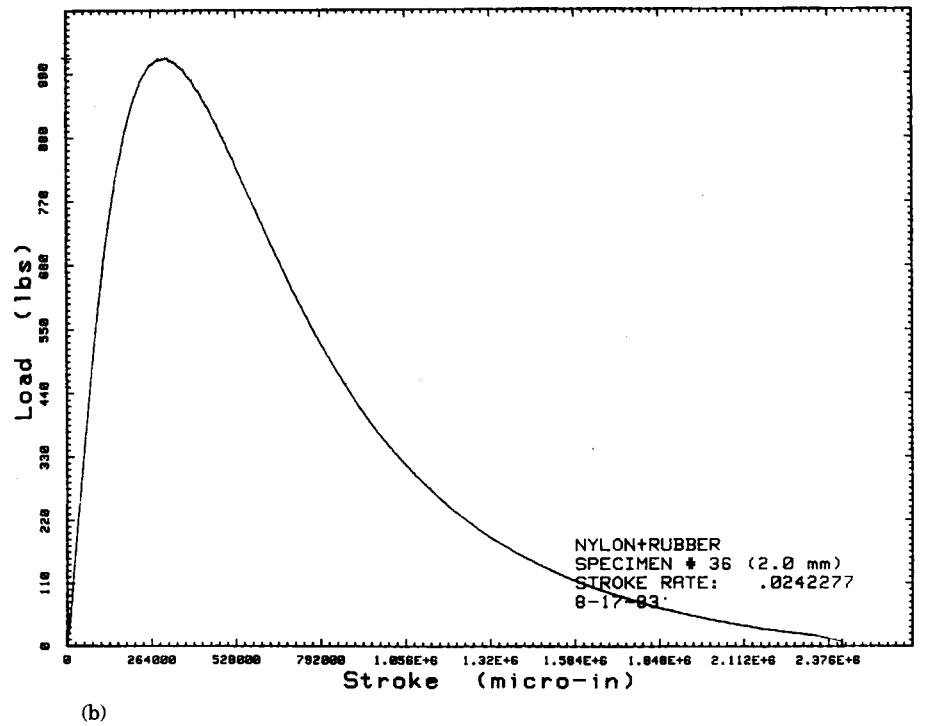

(b)

Fig. 3. Typical load-displacement curves obtained from compact tension tests of (a) N66 (b) N66ST (c) N66-G13 and (d) N66-G33.

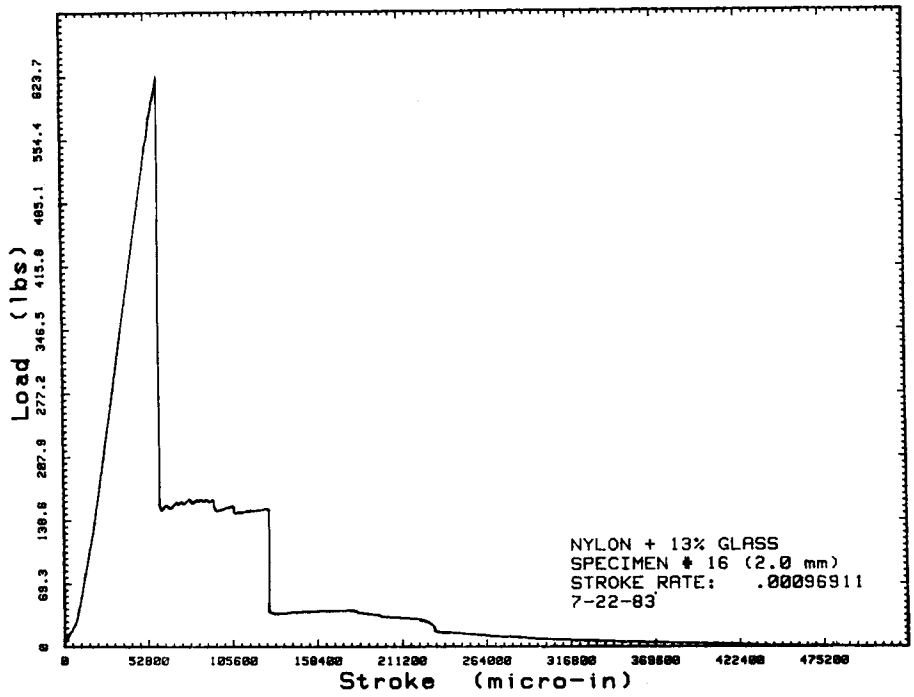
Load (lbs)
0
69.3
138.8
207.9
277.2
346.5
415.8
485.1
554.4
623.7
0
52800
105600
158400
211200
264000
316800
369600
422400
475200
Stroke (micro-in)
NYLON + 13% GLASS
SPECIMEN # 16 (2.0 mm)
STROKE RATE: .00096911
7-22-83

(c)

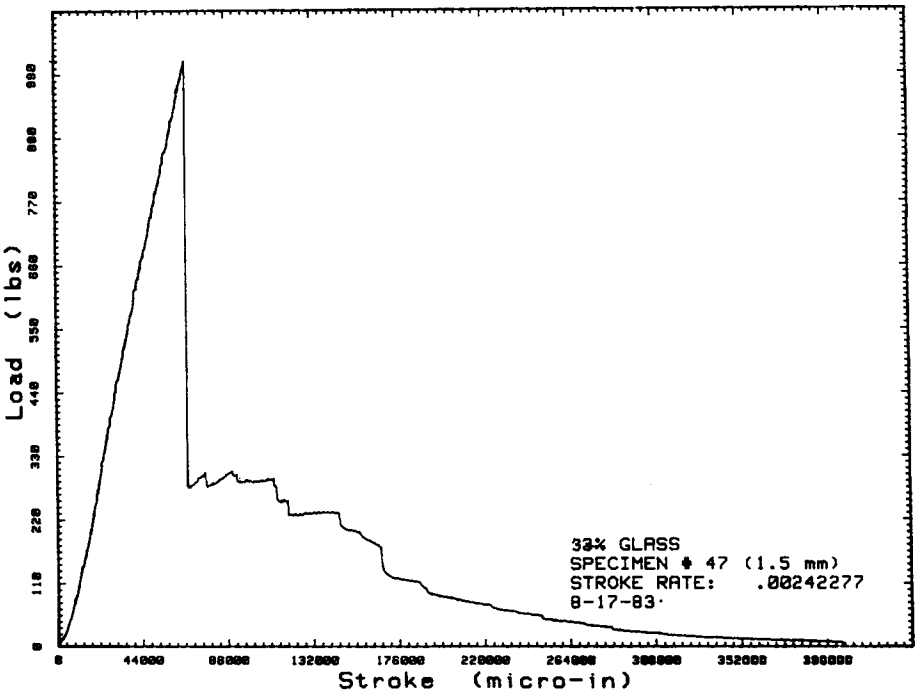
Load (lbs)
0
110
220
330
440
550
660
770
880
990
0
44000
88000
132000
176000
220000
264000
308000
352000
396000
Stroke (micro-in)
33% GLASS
SPECIMEN # 47 (1.5 mm)
STROKE RATE: .00242277
8-17-83

(d)

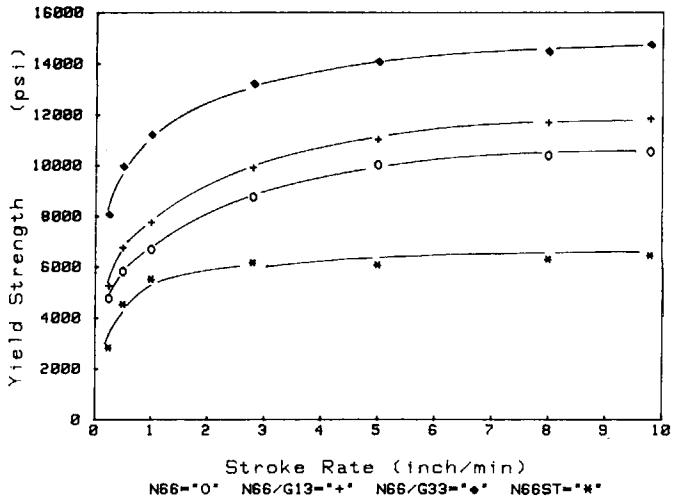

Fig. 4. The yield strengths of N66, N66ST, N66-G13, and N66-G30 in relation to the loading rate.

was not studied. It may be noted that Haskell et al.[13] observed a slight notch depth dependency of K_Q for carbon-fiber–reinforced PC and Lee et al.[14] showed that the K_Q values of epoxy appeared to be independent of the notch depth. The difference between these observations has yet to be resolved.

The stroke rate had a large effect on the mechanical behavior; both the R_{SC} and K_Q decreased as the stroke rate increased. Figure 5 shows that, for constant strain rates, the specimen strength ratio R_{SC} changed very little by adding 33% glass fiber to Nylon 6/6 but decreased by about one-third by adding in only 13% glass fiber. A factor of 2.5 times increase in R_{SC} was observed if the nylon matrix was modified by adding an elastomer phase. Since R_{SC} is proportional to (P_{max}/σ_y), the above observations suggested that the 13% glass fiber nylon was not able to support a load proportional to its higher yield strength. In the 33% glass fiber nylon, P_{max} increased at about the same rate as σ_y, resulting in little change in R_{SC}. This implied that fracture resistance of N66-G13 was inferior to that of unreinforced

TABLE 2
Effects of Notch Depth on K_Q and R_{SC}

Material	Notch depth (mm)	K_Q (lb.-in.$^{-3/2}$)	R_{SC}
PES-G30	0.25	11,280	0.09
	0.50	17,754	0.130
	0.75	21,069	0.160
	1.00	18,832	1.40
N66	1.00	11,203	3.15
	1.25	10,008	2.85
	1.50	10,316	2.95
	1.75	9,440	2.75
	2.25	10,755	3.15

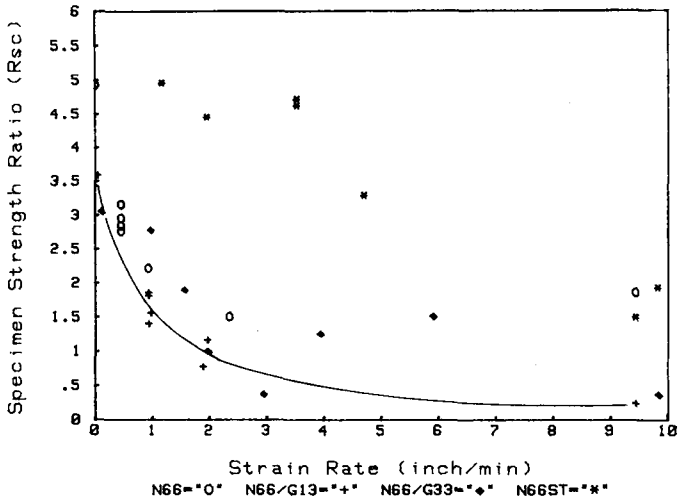

Fig. 5. The specimen strength ratios as a function of strain rate.

N66 (the 13% glass fibers did not provide beneficial effects to resist crack nucleation and propagation); N66-G33 appeared superior in crack resistance (33% glass fibers played a positive role in this case). However, this advantage gradually disappeared as the strain rate increased, as indicated by the trend for the R_{SC} to converge to that of unreinforced, unmodified nylon matrix (Figure 5). This is best illustrated by the fact that the K_Q values of both reinforced nylons appeared to converge to K_Q of Nylon 6/6 as the strain rate was raised (Figure 6). The reduction in K_Q of the polymers studied with the increased loading rate will be explained in the next section on the basis of crack propagation mode observation. For the rubber-toughened nylon, the higher maximum tensile load (P_{max} combined with the lower yield

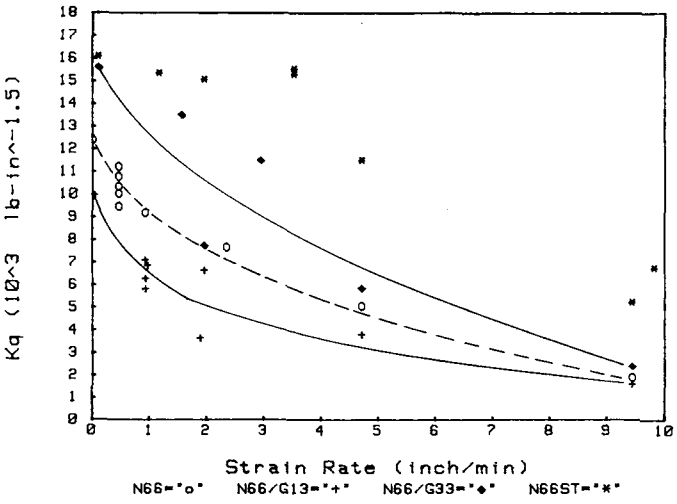

Fig. 6. The strain rate dependency of fracture toughness of Nylon 6/6-based polymers.

strength σ_y resulted in a higher specimen strength ratio and fracture toughness K_Q. Under all testing conditions utilized in the present investigation, N66ST was much tougher and more ductile than fiber reinforced and unreinforced nylon. The matrix type appeared to play a dominant role in resisting crack propagation.

A typical load-displacement curve of compact tension PES-G30 sample is shown in Figure 7(a), and the loading rate dependency of K_Q is presented in Figure 7(b). Again, the fracture toughness of fiber reinforced poly(ether sulfone) is highly dependent upon the strain rate. This is also reflected by a change in crack propagation mode, to be discussed next.

Crack Propagation Mode

The specimens for crack propagation mode study were rectangular bars normally used in three-point bending test. A single edge notch of depth ⅛ in. was first machined by a double-angle cutter from each bar to serve as a starting crack. One surface of each bar was then metallographically polished with sufficient care to minimize the fiber damage. After the surface is prepared and inspected at high magnification, a crack is grown in the desired direction by flexural loading (Figure 8). The crack growth at a normal Instron crosshead rate ($\leq$20 in./min) was generally stable, so that the crack growth can be terminated before complete failure ensues. The crack tip was then observed using a light microscope or scanning electron microscope. For each sample, the crosshead speed was varied between 0.01 and 20 in./min. Also, in order to examine each specimen under a very high test rate, a Charpy impact test was performed on each polymer type.

Figures 9A and B illustrate the crack propagation mode at relatively low magnification in PES-G30 and N66-G33, respectively. Cracks in all the reinforced plastics studied appeared to propagate in such a manner as to avoid most of the fibers when the loading rates were low (e.g., slower than 5 in./min). A slightly higher magnification version of Figure 9B is shown in Figure 9C while the corresponding fracture surface of this specimen presented in Figure 9D. Although the fiber avoidance mode appears to operate at these low strain rates, interaction of the crack with fibers does happen, resulting in some debonding (especially near the fiber end), which can be seen in the planar view (Figure 9A–C), and some pulled-out or broken fibers as visible on the fracture surface (Figure 9D).

Figure 9 and subsequent micrographs indicate that the fibers tend to agglomerate into small groups, roughly parallel in orientation. Observation of all reinforced materials under low-rate loading reveals that the crack follows a path that avoids these clustered fiber groups as much as possible, leaving a zigzag appearance in the micrographs of low magnification. The high depth of field of scanning electron microscopy (SEM) does allow us to observe that the planar zigzag path on the surface is repeated in the thickness direction as well. Thus a crack front does not seem to define a flat plane, but instead moves locally in different directions at different positions through the thickness, depending on the local fiber arrangement. The various parts of the crack front seem to eventually join together to form a continuous zigzag path by breaking away any material between the local growth regions.

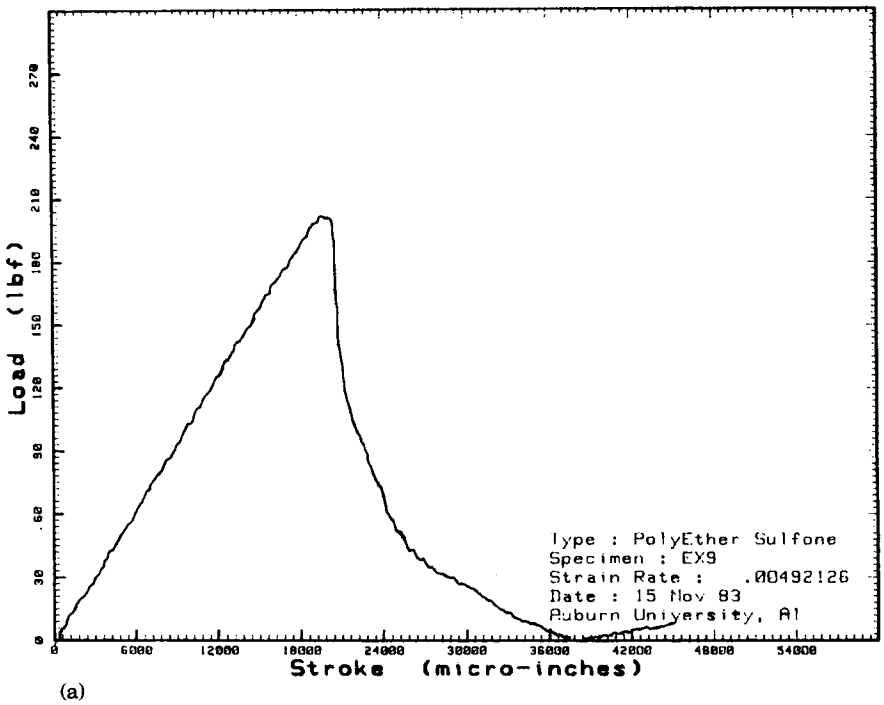

(a)

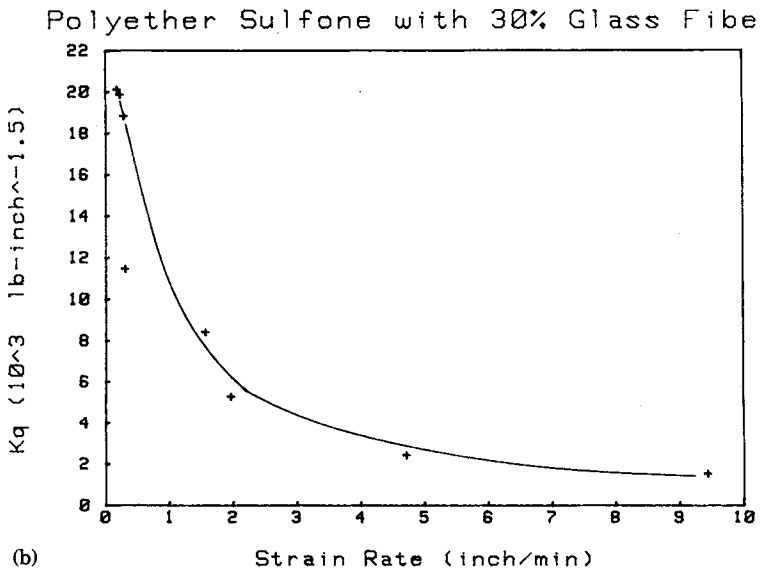

(b)

Fig. 7. (a) A typical load-displacement curve of compact tension specimen of PES-G30 and (b) the strain rate dependency of PES-G30 fracture toughness.

The loading rate was observed to have a profound effect on the crack propagation mode. At higher test rates the zigzag is not as noticeable as it is at low rates. As the test rate is increased, the crack path appears flatter and the fiber-breaking tendency becomes more pronounced. This tendency may be illustrated in the SEM micrographs of Figure 10, which show the planar view of crack growth mode in N66-G33. Figure 10A shows that, at

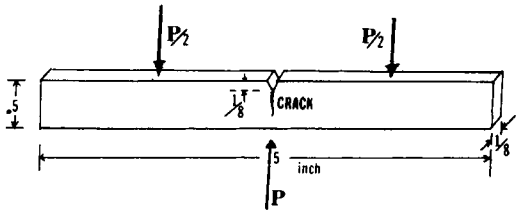

Fig. 8. Schematic of flexural loading specimen utilized for crack propagation mode observation.

a crosshead rate of 0.1 in./min, the crack path was highly zigzagged to avoid fiber clusters. However, fiber debonding and breaking appear to operate as well despite the loading rate being relatively low. As the rate was increased to 1 in./min. (Fig. 10B), both the degree of crack zigzagging and of fiber debonding were reduced while the frequency of fiber breakage was increased. This fiber-breaking phenomenon was more apparent in Figure 10C (10 in./min.), where the crack appeared very flat. As shown in Figure 10D, the fast-growing crack due to impact loading has essentially broken all the

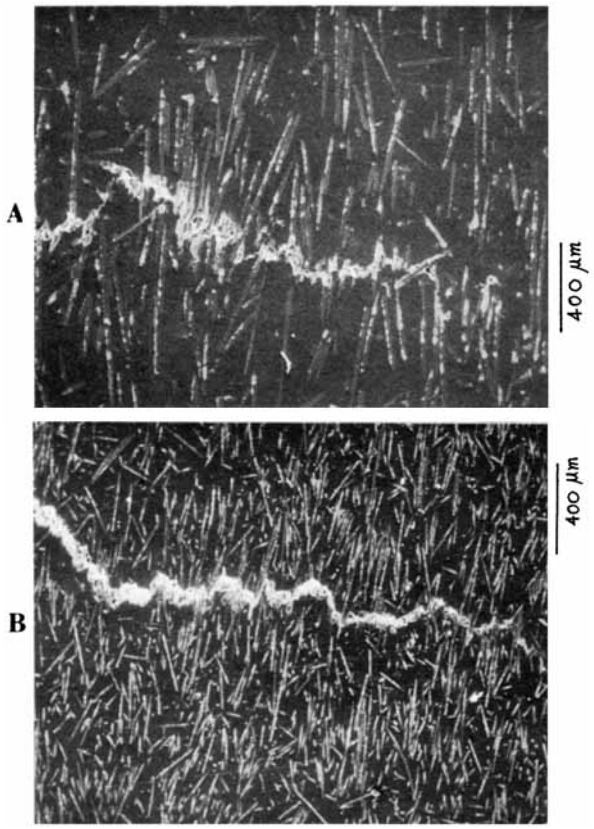

Fig. 9. Scanning electron micrographs showing the crack propagation mode. (a) PES-G30 with loading rate 0.05 in./min. (b) N66-G33 with loading rate 0.5 in./min. (c) Same as (b) but at higher magnification. (d) Same as (b), after fracture.

fibers on a flat plane. No crack zigzagging or fiber-avoidance mode could be identified. That the degree of debonding decreased with increased loading rate may be further illustrated in the SEM fractographs of Figure 11. The fracture surface of N66-G33 loaded at 0.5 in./min. (Figure 11A) indicated that there exists a circular minute crack between each fiber and its surrounding matrix, very much analogous to an electrical wire embedded in an overly large socket. Apparently, debonding has taken place between fibers and matrix during such a low-rate loading. Contrarily, clean fiber breakage occurred during impact loading, leaving behind fiber segments firmly embedded in the nylon matrix. No obvious interfacial debonding could be identified in Figure 11B. This observation applies to all the reinforced polymers studied. The implication of the crack propagation mode for the fracture toughness will be discussed later.

Interpretation of Fracture Data

Mandell and coworkers[3,10] have similarly observed the modes of crack propagation for injection-molded short glass and carbon-fiber–reinforced thermoplastics. The matrices ranged from ductile to brittle, with fiber contents varying between 30 and 40%. The main crack was found[3,10] to grow

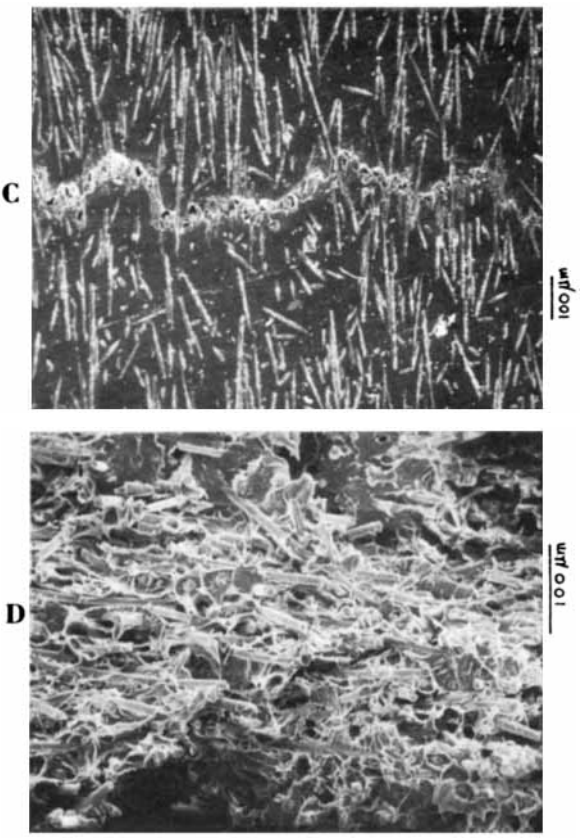

Fig. 9. (*continued from previous page*)

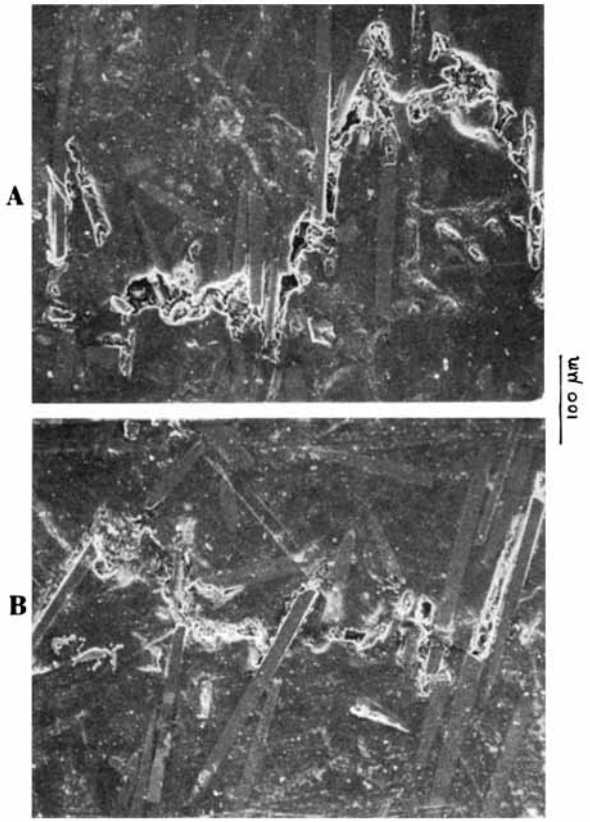

Fig. 10. SEM micrographs of crack propagation mode in NGG-G33. (a) loading rate = 0.1 in./min, (b) 1 in./min, (c) 10 in./min., and (d) after Charpy test.

in a fiber-avoidance mode, bypassing regions of agglomeration of locally aligned fibers. These workers[3,10] attempted to relate the fiber avoidance mode to fracture toughness by postulating that the crack should be able to propagate if the local stress reaches the ultimate tensile strength (UTS) at a critical distance γc, ahead of the crack tip, similar to the length of the longer fibers (l_f^*). The critical length l_f^* in the distribution was taken for convenience as the length exceeded by the top 5% of the fibers. The local stresses around the crack tip were given by[15]

$$\text{Local stresses} \cong \frac{K_I}{(2\pi r)^{1/2}} \tag{1}$$

where r is the distance from the crack tip. According to the hypothesis of Mandell et al.,[3,10] the crack will propagate when the local stress reaches the UTS at a critical radius r_c equal to the length of the longer fibers or agglomerations:

$$r_c = l_f^* \cong \frac{1}{2\pi}\left(\frac{K_I}{\text{UTS}}\right)^2 \tag{2}$$

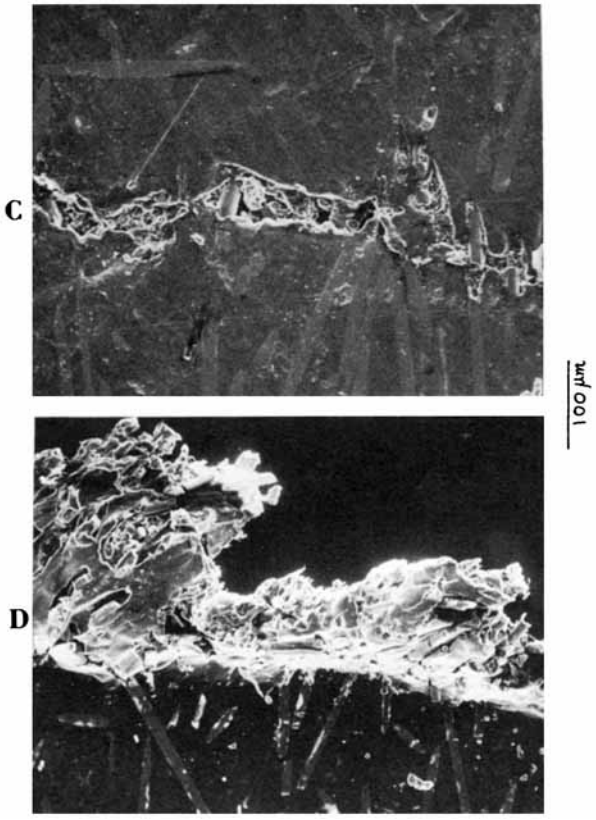

Fig. 10. (*continued from previous page*)

and at this condition K_I will be the fracture toughness K_Q, so that

$$K_Q \cong \text{UTS}\,(2\pi l_f^*)^{1/2} \tag{3}$$

This relationship appeared to be in agreement with the experimental data, although it may be noted that the loading rate of 0.5 cm/sec (11.4 in./min) was used throughout these two reports.[3,10] They stated that the great variation in matrix toughness and interfacial bond strength did not seem to greatly influence the fracture toughness of the reinforced thermoplastics studied. Any influence the constituent and interface properties did have was believed to have entered through the UTS.[3,10]

In order to determine the scope of applicability of this hypothesis, we have plotted the values of $(1/2\pi)\,(K_Q/\text{UTS})^2$ against the loading rate of reinforced polymers. According to this hypothesis [eq. (2) or (3)], this quantity is related to l_f^* and should remain constant irrespective of variation in loading rate. However, as shown in Figure 12, the magnitude of $(1/2\pi)\,(K_Q/\text{UTS})^2$ decreases with increasing test rate for both reinforced nylon samples (N66-G13 and N66-G33). This implies that the hypothesis proposed by Mandell et al.[3,10] cannot be valid without modification. It appears that the ef-

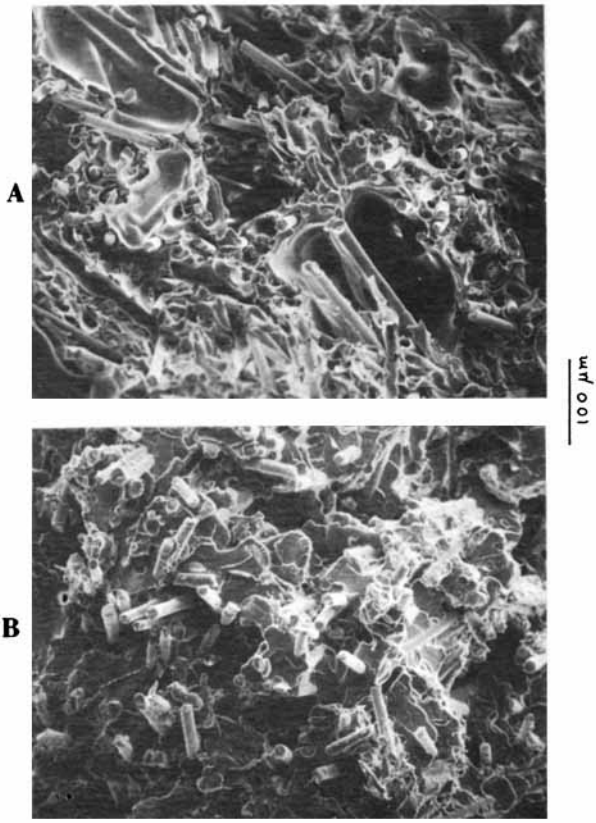

Fig. 11. SEM fracture surface morphology of N66-G33 (a) loaded at 0.5 in./min and (b) loaded at high rate (Charpy test).

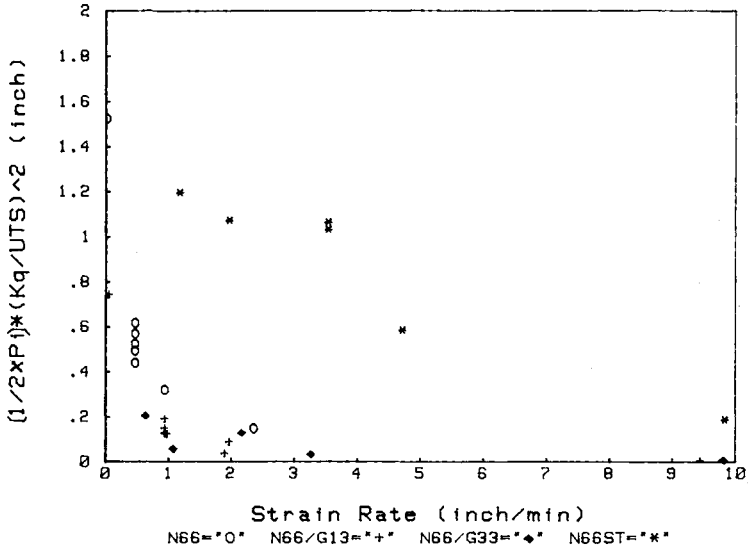

Fig. 12. The magnitude of $(1/2\pi)(K_Q/\mathrm{UTS})^2$ as a function of loading rate.

fective dimension of the fiber cluster zone that the crack would try to avoid is decreased with increased test rate. This is consistent with our observation that the degree of zigzagging was reduced if we raised the test rate. This would suggest that the effective l_f^* should vary with test rate if the hypothesis is to remain valid.

An alternative way to explain the fracture behavior is to consider the traditional approach, which concentrates on the fiber debonding energy and pullout friction.[16] As evident from our crack propagation mode observation and fracture surface study, the possible sources of fracture toughness are (1) fiber avoidance mode, which requires the crack to grow through a longer distance and thereby dissipate a greater amount of energy in creating new surfaces, (2) interfacial debonding and the subsequent pullout friction, and (3) the simple breakage of fibers in the crack path.

At low test rates all three mechanisms are believed to operate, although mechanisms 1 and 2 appear to dominate. Under such loading rates the crack will have sufficient time to find an easier way to propagate while allowing debonding and fiber pullout to operate. Both 1 and 2 are responsible for the greater fracture toughness K_Q observed at low test rates. When the test rate was high, the material had to cooperate to accommodate a rapid elongation, leading to fast cracking on a flatter plane. In this case, the fiber avoidance mode was minimal and the time scale was too small to allow for appreciable extent of fiber debonding and pullout. The fracture resistance arose solely from the need to cleave the matrix and fibers in the flat pathway of crack. The fracture toughness was therefore relatively low for reinforced thermoplastics subjected to high-rate loading. That the fracture toughness K_Q of N66-G13 and K_Q of N66-G33 approach asymptotically that of unreinforced N66 at high loading rates indicates that simple fiber breakage does not require much more energy than does flat matrix cleavage of comparable area. The fracture behavior of reinforced thermoplastics is therefore matrix dominant at high rates.

CONCLUSION

The fracture behavior of several glass-fiber–reinforced and unreinforced thermoplastics has been studied. It has been demonstrated that the ASTM E399 standard method proposed to measure the plane strain fracture toughness of metallic materials may also be used, with appropriate modification, to characterize the fracture behavior of reinforced polymers. It was discovered that the crack in the short fiber reinforced polymers tends to grow in such a manner as to avoid the agglomerations of fibers at low test rates. However, the fiber debonding and pullout friction play an important role in contributing to fracture resistance as well. Increasing the test rate tends to reduce the importance of fiber avoidance mode, resulting in a flatter and straighter crack growth path. The degree of fiber debonding and pullout friction was reduced as well, leading to a decrease in fracture toughness. Under high test rates, the frequency of fiber breakage is high, which, however, contributes very little to the fracture resistance. The failure behavior of reinforced polymers at high loading rates appears to be dominated by the matrix properties.

Financial support for this project was provided by Auburn University Engineering Experiment Station. This support is gratefully acknowledged. We also thank Mr. Y. S. Chang for assistance on technical drawing.

References

1. J. F. Mandell, D. D. Huang, and F. J. McGarry, *Polym. Composites,* **2**, 137 (1981).
2. J. F. Mandell, F. J. McGarry, D. D. Huang, and C. G. Li, *Polym. Composites,* **4**, 32 (1983).
3. J. F. Mandell, D. D. Huang, and F. J. McGarry, in *Short Fiber Reinforced Composite Materials,* ASTM STP #772, Philadelphia, 1982, p. 3.
4. B. F. Blumentritt, B. T. Vu, and S. T. Cooper, *Polym. Eng. Sci.,* **14**, 633 (1974) and **15**, 428 (1975).
5. V. R. Riley, *J. Compos. Mater.,* **2**, 436 (1968).
6. H. Fukuda and T. W. Chou, *J. Mater. Sci.,* **16**, 1088 (1981).
7. M. Taya, J. Compos. Mater. 15 (1981) 198.
8. P. T. Curtis, M. G. Bader, and J. E. Bailey, *J. Mater. Sci.,* **13**, 377 (1978).
9. N. Sato, T. Kurachi, S. Sato, and O. Kamigaito, *J. Mater. Sci.,* **19**, 1145 (1984).
10. J. F. Mandell, A. Y. Darwish, and F. J. McGarry, in *Test Methods and Design Allowables for Fibrous Composites,* ASTM STP 734, C. C. Chamis, Ed., Amer. Soc. for Testing Mat., Philadelphia, 1981, pp. 73–90.
11. J. M. Schultz and K. Friedrich, *J. Mater. Sci.,* **19**, 2246 (1984).
12. E-399 Plane Strain Fracture Toughness of Metallic Materials, Annual Book of ASTM Standards, Amer. Soc. Testing Mater., Philadelphia, 1981.
13. W. E. Haskell, III, S. P. Petrie, and R. W. Lewis, *Polym. Eng. Sci.,* **23**, 14 (1983).
14. C. Y. C. Lee and W. B. Jones, *Polym. Eng. Sci.,* **22**, 1190 (1982).
15. J. F. Knott, *Fundamentals of Fracture Mechanics,* Butterworths, Boston, 1973, p. 133.
16. A. Kelly, *Strong Solids,* 2nd Ed., Clarendon Press, Oxford, 1973, p. 157.

Received Jaunary 10, 1985
Accepted February 25, 1985